

# Fundamental processes governing operation and degradation in state of the art P-OLEDs

Matthew Roberts<sup>\*a</sup>, Kohei Asada<sup>b</sup>, Michael Cass<sup>a</sup>, Chris Coward<sup>a</sup>, Simon King<sup>a</sup>, Andrew Lee<sup>a</sup>,  
Martina Pintani<sup>a</sup>, Miguel Ramon<sup>a</sup>, Clare Foden<sup>a</sup>

<sup>a</sup>Cambridge Display Technology Ltd, Greenwich CDT Ltd Head Office, Building 2020, Cambourne Business Park, Cambridgeshire, CB23 6DW;

<sup>b</sup>Sumitomo Chemical Co., Ltd, 6 Kitihara, Tsukuba, Japan 300-3294

## ABSTRACT

We present a theoretical and experimental analysis of operation and degradation of model fluorescent blue bilayer polymer organic light emitting diodes (P-OLED). Optical and electrical simulations of bilayer P-OLEDs are used to highlight the key material and device parameters required for efficient recombination and outcoupling of excitons. Mobility data for a model interlayer material poly(9,9-dioctylfluorene-N-(4-(2-butyl)phenyl)-diphenylamine) (TFB) and a model fluorescent blue light emitting material poly-(9,9'-dioctylfluorene-co-bis-N, N'-(4-butylphenyl)-bis-N,N'-phenyl-1,4-phenylenediamine) (95:5 mol%) (F8-PFB random copolymer), is shown to satisfy the key charge transport characteristics required to ensure exciton formation at the optimum location for efficient extraction of the light where  $\mu_h(\text{LEP}) < \mu_e(\text{iL}) < \mu_e(\text{LEP}) < \mu_h(\text{iL})$ . A method to measure the photon generation zone profile and dipole orientation is presented and shown to follow the expected behavior. The efficiency drop of P-OLEDs during device operation is a known issue, the understanding and prevention of which is key for the commercial success of P-OLED technology. We present a detailed degradation study of devices containing model materials, and highlight the generation of fluorescence quenching sites as the key factor limiting the operational stability. A striking feature of this degradation is its partial (~50%) reversibility upon baking above the LEP glass transition temperature. Some reversibility is also observed in the conductivity, suggesting a common origin to the optical and electrical degradation. We also show that the species responsible for the generation of the reversible PL quenching sites are the excitons themselves, and that optically excited excitons can also generate many of the features characteristic of electrical stressing. Finally we demonstrate that materials with a dramatically improved lifetime also suffer from a similar, although slowed down, degradation mechanism, where the reversible component is increased to almost all (>90%) of the quenching sites produced. This highlights the importance of understanding these reversible phenomena in improving P-OLED lifetime and commercial adoption of the technology.

**Keywords:** Polymer, LED, polyfluorene, device models, efficiency, mobility, degradation, lifetime, reversible

## 1. INTRODUCTION

The efficiency and lifetimes of P-OLEDs has increased dramatically over the past decade, with efficiencies of fluorescent blues now achieving 8cd/A at CIEy=0.21 with lifetimes > 25,000hrs from 1000cd/m<sup>2.1</sup>. There has been extensive use of both optical<sup>2</sup> and electrical<sup>3,4</sup> models to describe and optimize device efficiency in OLEDs, but for polymer OLED devices these models have mainly concentrated on simple structures consisting of just one light emitting polymer (LEP) layer<sup>5</sup>. The basic device structure has remained relatively simple throughout this time apart from the introduction of an interlayer<sup>6</sup> (iL) between the LEP and hole injection layers (HIL), giving a bilayer structure which has been shown to improve both the efficiency and lifetime of P-OLEDs<sup>7</sup>. There have also been extensive studies into the degradation of polyfluorene and its derivatives, often concentrating on factors influencing its stability to photooxidation<sup>8</sup>. There is remarkably little in the literature on the electrical and optical modeling of bilayer P-OLED devices, and less still on the degradation of fluorene-amine based copolymer devices, which is the subject of this study.

This paper is organised as follows; Section I covers the bilayer device structure, model iL and LEP materials, and presents the electrical and optical models used for simulating the exciton formation and outcoupling efficiency. The key material and device parameters required to generate efficient recombination in the appropriate position for outcoupling

\*mroberts@cdtld.co.uk; phone 44 (0)1954 713685; fax 44 (0)1954 713628; cdtld.co.uk

are highlighted. In Section II we describe some material and device measurements in support of our main model assumptions and predictions. In particular we pay attention to charge mobility and injection efficiency into the model materials set, where it is argued that the conditions required for hole accumulation and exciton recombination at the LEP:iL interface are satisfied. PGZ and dipole orientation measurements are shown to be in good agreement with our expectations. Section III describes the changes observed on accelerated lifetesting of model devices, and highlights the generation of fluorescence quenching sites in the fluorene-amine copolymer as the dominant degradation mechanism. Further observations on causes and characteristics of these quenching sites are presented. We highlight that this degradation mechanism can be caused by electrical or optically excited excitons, is partially reversible upon baking above the LEP glass transition temperature, and that this reversible character is much more dominant in an improved materials set. Conclusions are summarised in Section IV.

## 2. MODELLING: DESIGN RULES FOR HIGH EFFICIENCY

### 2.1 Materials and device structure

Figure 1 shows the basic device structure and model materials used in this study. The transparent conductive HIL similar in function to PEDT:PSS is spun on top of a patterned ITO coated glass substrate. The interlayer material (iL) is an A-B copolymer of F8 and TFB (poly (9,9-dioctylfluorene-N-(4-(2-butyl)phenyl)-diphenylamine), which we will call TFB. The TFB interlayer is formed by spin coating from ~1% xylene solution and baking at 180C for 1 hour in a nitrogen purged glovebox, as described in the literature<sup>6</sup>. Subsequent rinsing with an organic solvent such as xylene leaves a thin ~15nm layer of reduced solubility upon which the LEP layer can be spin coated without significant intermixing. The LEP material is a random copolymer consisting of 95% F8 and 5% PFB units (poly-(9,9'-dioctylfluorene-co-bis-N, N'-(4-butylphenyl)-bis-N,N'-phenyl-1,4-phenylenediamine) (95:5 mol%)). The cathode is thermally evaporated at a pressure of  $\sim 10^{-6}$  mbar and consists of a low work function material capped with aluminium.

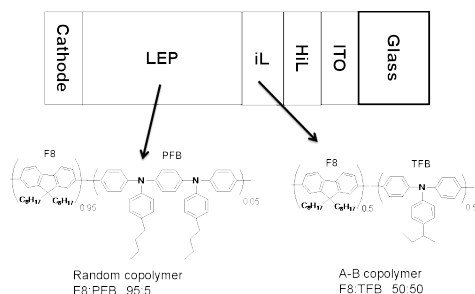


Figure 1. Device structure and model materials used in this study. The layer thicknesses are approximately ITO(45nm), HIL(30nm), iL(15nm), LEP(55nm), cathode (200nm).

### 2.2 Optical model : Design rules for high efficiency

An optical model is used to understand the main factors governing the outcoupling efficiency. The model used is based on a scattering matrix method to solving Maxwell's equations for the power loss spectrum of a forced oscillating dipole within a multilayer structure<sup>9</sup>. In addition to all cavity layer thicknesses and optical constants (dispersive and anisotropic if required), the model takes as inputs the dipole wavelength, orientation and position within the cavity. We have determined the optical constants of all the materials used within our devices using a J.A Woollam Co. M-2000 diode array rotating compensator spectroscopic ellipsometer. The technique for the polymer layer involves simultaneous fitting of reflection and transmission ellipsometric data at a series of angles, following the method described by Ramsdale and Greenham<sup>10</sup>. As outputs, the model provides the modification to the dipole radiative rate and the relative power lost into modes of any given wavevector. This includes the surface escape modes, as well as all cavity modes (energy lost to plasmons/metal absorption, guided within P-OLED stack or trapped within the glass substrate). To account for the broad emission spectrum of P-OLED materials, deviations for isotropic dipole orientation, and distributions of emitting dipole positions within the cavity, all wavelengths, orientations and positions are calculated and stored in a database, allowing a weighted sum of the model output to be computed depending on the user defined inputs. The weighting procedure is similar to that described in detail by Lu et al<sup>2</sup>.

Some example results are shown in figure 2, to illustrate some of the key factors governing device design. Of particular importance is for a dipole to be in-plane, and to be in a position of maximum constructive interference with its reflections from the cathode (~55nm thick LEP for a blue emitter with peak wavelength 460nm, refractive index 1.75). Nearly all perpendicular dipoles will be waveguided within the device stack and eventually absorbed by the cathode, unless sophisticated scattering methods are employed<sup>11</sup>. Interestingly, the optimum distance from the cathode for perpendicular dipoles is in antiphase with the parallel dipoles, mainly due to the polarization dependent phase change at the cathode interface. This effect can be exploited to give a method of measuring the average dipole orientation (see section 3.6). We can also clearly observe quenching effects at both electrodes, due to coupling to short lived excitations at the electrode surfaces<sup>12</sup>. This study clearly suggests that the optimum PGZ is ~55nm from the cathode for maximum outcoupling, and >10nm from anode, to prevent excitons diffusing to the anode quenching zone. This can be achieved by choosing the appropriate layer thickness for the LEP and iL. Other general design rules are to maximize the cathode reflectance and fine tuning of the cavity by varying the optical thickness and reflectance properties of the anode layers (HIL and ITO).

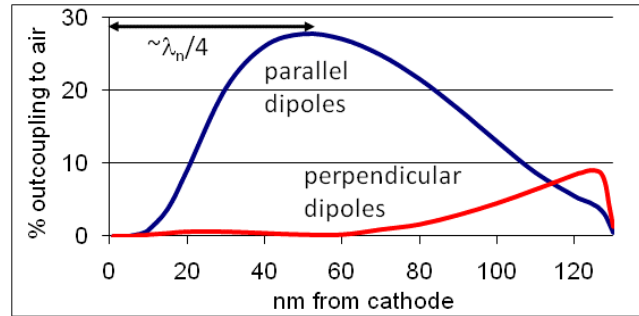


Figure 2. Outcoupling efficiency for blue excitons (weighted average over PL emission spectrum) as a function of dipole position and orientation within a 130nm thick LEP layer (no iL).

### 2.3 Electrical model : Design rules for high efficiency

The drift-diffusion equations are solved self-consistently in 1D in a similar fashion to that outlined by Barker et al<sup>13</sup> and Martin et al<sup>14</sup>. The equations reduce to a 2 point boundary value problem for which a variety of standard numerical solver routines exist. A Poole-Frenkel style field dependent mobility and the simple Langevin equation for recombination of polarons are used in the model. Explicit charge trapping is neglected, keeping the model as simple as possible and minimising the number of adjustable fitting parameters.

Injection is treated using the Scott-Malliaras modification of Schottky barrier boundary conditions<sup>15</sup>. If the injection barrier is reduced to 0.25eV or less the Scott-Malliaras formulism is not strictly valid, however the JV characteristic obtained is the same as that given by an Ohmic boundary condition. While the JV characteristic is the same for a small barrier and Ohmic injection, the non-ideality of the small barrier case gives a more realistic description of the exciton formation efficiency. Hence we use the Scott-Malliaras boundary condition even in those cases where injection is approximately Ohmic. The interface between organic layers is treated using the Arkipov equations for hopping between different Gaussian distributions<sup>16</sup>. In general the energy offset between LEP and iL is sufficiently small (<0.3eV) that the offset has a negligible impact on the performance of the device.

We have looked at the mobility and injection criteria required to bring about recombination of charges at the optimum position for outcoupling, as suggested by the optical simulations in section 2.2. We propose the following three rules of thumb. Provided the barriers to charge injection are not prohibitively high (eg > 600meV), the exciton formation zone can be kept away from the cathode by ensuring that the hole mobility of the LEP is much less than the electron mobility in the LEP. The exciton formation zone can be kept within the LEP layer and away from iL:HIL interface by ensuring that the hole mobility in the interlayer is much greater than the hole mobility in the LEP. Finally, the electron leakage into the anode contact can be minimized by ensuring that the electron mobility in the interlayer is lower than the electron mobility in the LEP. These conditions may be summarized as follows:  $\mu_h(\text{LEP}) < \mu_e(\text{iL}) < \mu_e(\text{LEP}) < \mu_h(\text{iL})$ .

In order to illustrate the main features of our bilayer device model, Figures 3 and 4 plot sample outputs of the electrical model for following parameter set: LEP ( $\Phi_{\text{cathode}}=0.45\text{eV}$ ,  $\mu_{0e}=2.5\text{e-}11$  ( $\text{m}^2\text{V}^{-1}\text{s}^{-1}$ ),  $\mu_{0h}=1.5\text{e-}12$ ,  $\gamma_e=6.6\text{e-}4$ ,  $\gamma_h=3\text{e-}4$ ), iL

( $\Phi_{\text{anode}}=0.2\text{eV}$ ,  $\mu_{0e}=8.0\text{e-}9\text{ m}^2\text{V}^{-1}\text{s}^{-1}$ ,  $\mu_{0h}=3.0\text{e-}11$ ,  $\gamma_e=6.4\text{e-}4$ ,  $\gamma_h=5\text{e-}4$ ), Interface parameters (dielectric permittivity  $\epsilon=3$ , the density of hopping sites  $N_s=1\text{e}27\text{m}^{-3}$  and the width of the energy distribution  $\sigma=100\text{meV}$ ). We have chosen parameters that satisfy the conditions outlined in the previous paragraph and also serve to illustrate the main factors controlling the efficiency in this device structure.

First to note is that the exciton formation efficiency, defined as the fraction of injected charge pairs that form an exciton, is  $< 100\%$ . This is a result of the contacts not being treated as perfect ohmic interfaces, allowing for bipolar currents at the contacts. The effect shows up very clearly in cross sectional breakdown of the current density shown in figure 3. At low currents, when the electron conductivity is injection limited, the hole current dominates and reaches all the way to LEP:cathode interface, resulting in a broad PGZ and a significant hole current into the cathode electrode. As the voltage is increased, a combination of improved electron injection and higher electron mobility in the LEP improves the current balance, the hole current into the cathode drops and the exciton formation zone moves towards the anode side of the device. At 3V above  $V_{\text{bi}}$  we have close to the optimum situation for efficiency in terms of current balance and exciton formation zone. As the voltage is increased to very high levels, 6V above  $V_{\text{bi}}$ , the electron current starts to cross the  $i\text{L}$  and reach the anode contact, again contributing to a drop in the exciton formation efficiency.

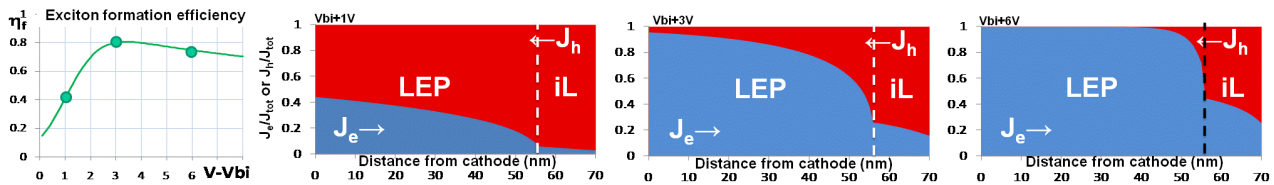


Figure 3. Exciton formation efficiency vs voltage (left) for a model bilayer device described by the parameters given in the text, along with normalized current density profiles at 1V, 3V and 5V above  $V_{\text{bi}}$ . The non ideality of the contacts and the mismatches in material mobilities result in holes flowing through to the cathode at  $V_{\text{bi}}+1\text{V}$ , and electrons flowing through to the anode at  $V_{\text{bi}}+6\text{V}$ . The best current balance is achieved near  $V_{\text{bi}}+3\text{V}$ .

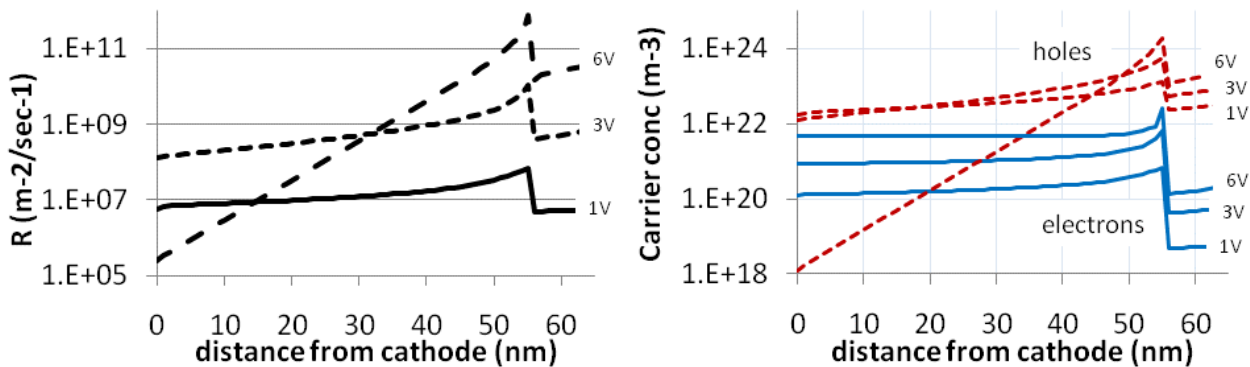


Figure 4. Exciton formation zone (left) and background charge density profiles (right) at 1V, 3V and 6V above  $V_{\text{bi}}$  for a model bilayer device described by the parameters in the text, illustrating that excitons recombine predominantly within the LEP at the  $i\text{L}:\text{LEP}$  interface at all voltages and that the hole density is the dominant charge building up at this interface.

Figure 4 shows how the exciton formation zone and background charge density profiles vary with applied voltage. It is notable that the exciton formation zone profile is located mainly within the LEP layer and peaks at the  $i\text{L}:\text{LEP}$  interface for all voltages, as desired for efficient outcoupling of the light. This shape of exciton formation zone profile, governed by the product of local electron and hole density, is dominated by and closely resembles the hole density profile. This effect can be understood as originating from the condition  $\mu_h(\text{LEP}) < \mu_e(i\text{L}) < \mu_e(\text{LEP}) < \mu_h(i\text{L})$ . In the limit of negligible charge injection barriers, the contrast of electron and hole mobility in the LEP ensures that hole density is much higher than the electron density within this layer, in particular in the region closer to the anode. Departures from ohmic injection at the cathode contact will only serve to enhance the asymmetry in the charge densities and further increase the dominance of the hole density. The very high hole mobility of the  $i\text{L}$  material ensures that the hole density does not build up sufficiently within this layer to dominate the recombination. The low electron mobility in the  $i\text{L}$  is designed to prevent the electron current leaking into the anode. This low  $\mu_e(i\text{L})$  does result in the buildup of electron

density and some undesired exciton formation within the interlayer. However, provided the iL electron mobility is not too low, the fraction of excitons formed within the interlayer remains small relative to the fraction formed within the LEP layer.

We conclude this section by summarizing the key design rules for high efficiency suggested by our optical and electrical models in figure 5.

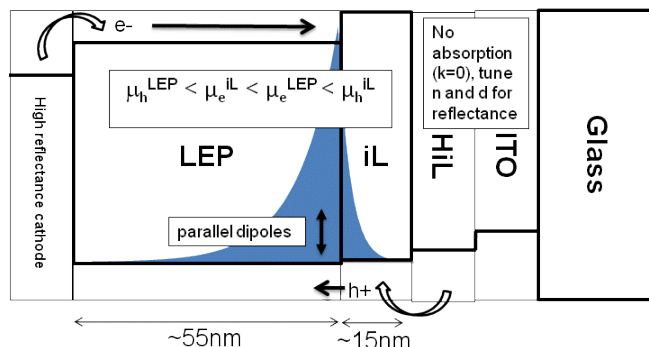


Figure 5. Schematic of optimized material mobility and thickness design rules. The desired shape of exciton formation zone is achieved by ensuring adequate charge injection, and that the material mobilities obey the trend specified. The efficient outcoupling of the light is achieved by choosing a reflective cathode, 55nm LEP layer thickness, >10nm iL thickness, parallel dipoles, and careful design of the anode reflectance to maximize weak cavity effects.

### 3. EXPERIMENT: MATERIAL AND DEVICE CHARACTERISATION

#### 3.1 Hole mobility measurements

The requirement for the hole mobility to be much lower in the LEP compared to the iL is shown to be satisfied in our model materials by the time of flight hole mobility results for these materials shown in Figure 6. The TFB interlayer has over 5 orders of magnitude higher mobility than the LEP copolymer. Also shown is the literature value for the hole mobility of F8<sup>17</sup>. This suggests that the low percentage of amine units in the 95%F8:5%PFB copolymer LEP are acting as hole traps, consistent with the interpretations of van Mensfoort<sup>18</sup> and Khan<sup>17</sup>, and also consistent with the significant HOMO offset between the F8 (~5.8eV) and the PFB (~5eV) as measured by UV ionization spectroscopy. We have confirmed the low hole mobility values of the LEP model material with transient methods on hole only devices with layer thickness variations much closer to those found in devices (40-130nm). The Dark Injection Transient Spectroscopy (DITS) measurements were obtained following the method described by Campbell et al<sup>19</sup> and the differential susceptance (-ΔB) measurements were obtained following the method described by Martens et al<sup>20</sup>

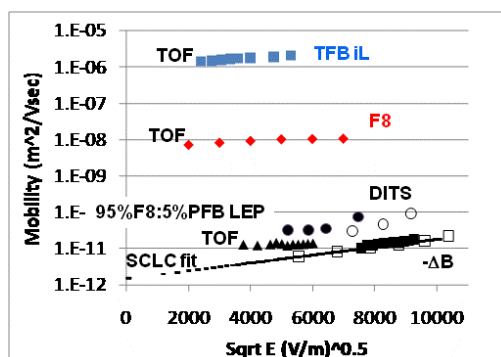


Figure 6. Hole mobilities of model materials. Time of flight (TOF) values for TFB, F8 and the LEP copolymer confirm > 5 orders of magnitude difference in hole mobility between LEP and iL. The low values of the amine copolymer hole mobility are confirmed with a number of other transient measurement techniques on hole only devices with a range film thickness and spin coating conditions applicable to devices (DITS in circles, differential susceptance in squares, SCLC fitting shown by dashes).

### 3.2 Hole injection barrier estimates

Comparison of measured versus modelled space charge limited currents using measured mobilities can yield an estimate of the injection efficiency, following the analysis of Fong et al<sup>21</sup>. These results are shown for both the LEP and iL materials in figure 7. For the LEP copolymer with low mobility the agreement is good, suggesting that the hole conduction in this material is space charge limited. For the TFB iL, the measured conductivity is 2-3 orders of magnitude lower than expected, suggesting that the injection at the HIL:TFB interface is not ideal, consistent with reports in the literature<sup>21,22</sup>. It is clearly much easier to satisfy the space charge limited injection criteria for a low mobility material compared to a high mobility material.

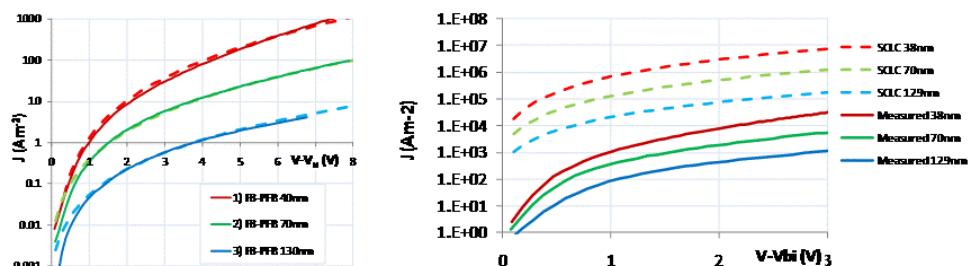


Figure 7. Hole only device conductivity (solid lines) vs SCLC model using TOF mobilities (dashed lines). The hole only devices have an aluminium cathode, and single layers of approx 40, 70 or 130nm layer of either LEP (left) or TFB (right). These results suggest that the hole conductivity of the LEP layer is space charge limited, whereas the TFB layer is injection limited.

We have tried to fit the TFB hole only device (HOD) data with mobilities more like the TOF results, and with a Scott Malliaras type barrier to hole injection. However, the fits obtained are very poor, and suggests that the non ohmic nature of this contact is not consistent with a simple barrier to injection. The only combination of parameters that can give a reasonable fit with our data occurs if we include a small barrier to hole injection and a TFB hole mobility that is 2 orders of magnitude lower than the TOF data (see figure 10). These are the parameters used at present in our simulations. This could reflect a real thickness dependence of the TFB mobility, or just highlight the current limitations to the model of charge injection at the HIL:TFB interface.

### 3.3 Hole conductivity and hole density in bilayer devices

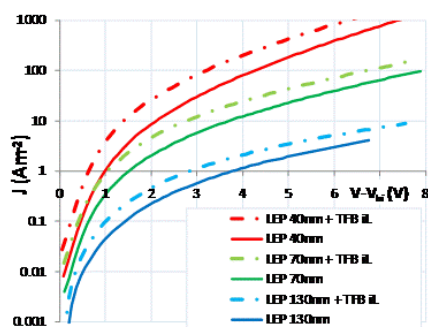


Figure 8. Hole only device JV traces of various thickness LEP with (dashed lines) and without (solid lines) the 15nm TFB interlayer. The conductivity improves by a factor ~2 for all thicknesses, suggesting that the conductivity within the LEP layer is predominantly space charge limited, despite the non-ideal HIL:TFB contact.

In order to check whether the non-ideal HIL:TFB interface affects the space charge limited conductivity characteristic of the LEP layer, we compare the conductivity of hole only device both with and without the 15nm TFB interlayer over a range of LEP thicknesses, shown in figure 8. Surprisingly, the current density increases slightly (factor of ~2) in all cases, suggesting that the hole conduction through the LEP is still predominantly space charge limited, and that the interlayer either slightly improves hole injection barrier into the LEP or increases the effective area of the anode contact.

It would appear that the non ideality of the HIL:TFB interface is not dramatically limiting the device conductivity, due to the particularly low hole mobility of the LEP having only a moderate demand of the hole supply from the injecting contact. Further simulations on bipolar device (not shown) suggest that the main impact of the non ideal injection at the HIL:TFB interface is to affect the small buildup of hole space charge within the iL. The impact on the hole buildup within the LEP layer, the exciton formation efficiency and formation zone profile, remain largely unaffected.

In order to test our model predictions on the hole space charge buildup, we carried out excited state absorption measurements on hole only devices. Changes in reflected light from a tunable wavelength source (white light+monochromator) induced by modulating the HOD device drive voltage from 0V to a target voltage V at 5KHz is measured using a Si photodiode and a lock-in amplifier. Figure 10 shows an excited state absorption spectrum of a hole only device biased at -15V, 10V and 15V. The sub band gap feature centred around 550nm is assigned to the radical cation in the LEP

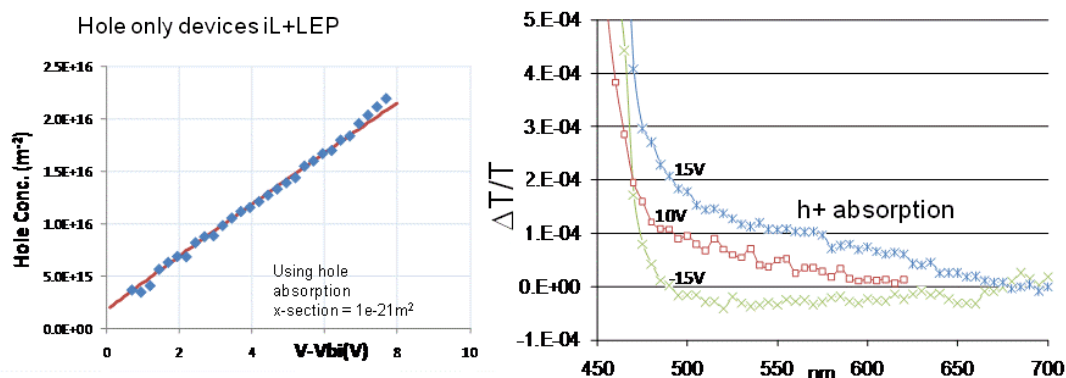


Figure 9. Hole absorption data for a bilayer hole only device (15nm TFB, 60nm LEP), The broad feature centred around 550nm is assigned as a radical cation. The linear growth of this feature with voltage is in agreement with the predictions for a space charge limited conductivity. Comparison with the electrical model output yields an estimate of  $1\text{E-}17\text{cm}^2$  for the hole absorption cross section.

If the wavelength is fixed at 550nm and we vary the modulating target voltage, we find a linear growth of this feature with voltage, in agreement with the theoretical estimates of space charge limited conductivity. If we attempt to fit the reflectance data to the hole concentration summed from the electrical model as shown in figure 9, we obtain a value for the absorption cross section of  $1\text{e-}17\text{cm}^2$ . This is within an order of magnitude of the literature values for radical cations of tetraphenylphenylenediamine<sup>24</sup> ( $7\text{e-}17\text{cm}^2$ ).

In summary, we conclude that the hole conductivity of our bilayer device is in good agreement with our simple model, with a significant hole density building up within the LEP layer, peaked at the iL:LEP interface, and increasing linearly with drive voltage. The exciton formation zone is expected to follow closely the shape of the hole density profile, which we are able to confirm in the section 3.5.

### 3.4 Electron conductivity measurements

The electron conductivity in amine-polyfluorene copolymer materials is believed to be dispersive and to show trapping behavior<sup>25</sup>, consistent with a stronger field dependence of the mobility. A full description of mobility requires extensive temperature and thickness dependent conductivity measurements and use of a sophisticated Gaussian disorder model. This treatment is beyond the scope of this work. However the simpler mobility models used in our simulations suggest that in order to bring about an exciton formation zone at the iL:LEP interface, the key factor is to ensure that  $\mu_h(\text{LEP}) < \mu_e(\text{iL}) < \mu_e(\text{LEP}) < \mu_h(\text{iL})$ . We demonstrate that these conditions are satisfied in our model LEP materials by extracting the electron mobility data from fitting of electron only device (EOD) data, as shown in figure 10. We choose cathode electrodes to have injection barriers  $<300\text{meV}$ , and obtain good fits for the electrical model over a range of LEP or iL thicknesses.

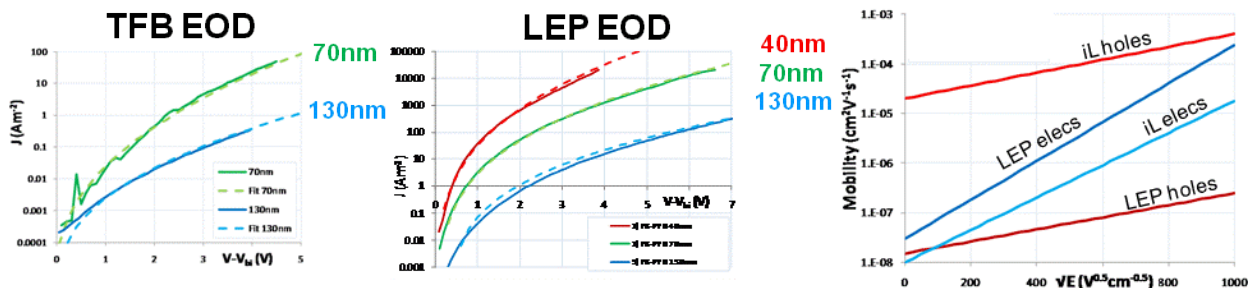


Figure 10. Electron only device data for a range of iL (left) and LEP (centre) material thicknesses. Solid lines show the experimental data, dashed lines show the fit with a barrier to injection <300meV. The values extracted show that at moderate fields, the electron and hole mobilities of the iL and LEP follow the trends recommended for high efficiency, namely  $\mu_h$  (LEP) <  $\mu_e$  (iL) <  $\mu_e$  (LEP) <  $\mu_h$  (iL).

### 3.5 Photon generation zone measurements

Most methods to determine the photon generation zone (PGZ) in P-OLED devices involve fitting the device emission spectrum to an optical model<sup>26,27</sup>. Here we follow a similar principle, where the s-polarized angular emission spectra for a 130nm LEP thick device are compared to the output of our optical model. The emission spectra are normalized to the spectrum at normal incidence to factor out any errors in the estimate of the cavity free emission spectrum. A hemisphere with diameter >10x the pixel width with its centre of curvature centred on the pixel is fixed with index matching UV curable epoxy to the substrate to enable access to the off-axis emission angles otherwise totally internally reflected within the glass substrate. For this LEP thickness the emission near the LEP:iL interface couples much more efficiently to the off axis modes, and the fit parameter becomes extremely sensitive to the PGZ profile. By choosing to use only the s polarized emission spectra, the PGZ fitting procedure becomes insensitive to the average dipole orientation, since we are only probing in-plane dipoles. For the fitting we describe the PGZ with a simple exponentially decaying function as shown in figure 11 so that the PGZ can be fit with just two free parameters, the characteristic width d (distance to 1/e) and peak position. Although we do not claim that this gives a unique fit, this functional form gives a good fit to the data and preserves the simplicity of the procedure without introducing unneeded complexity.

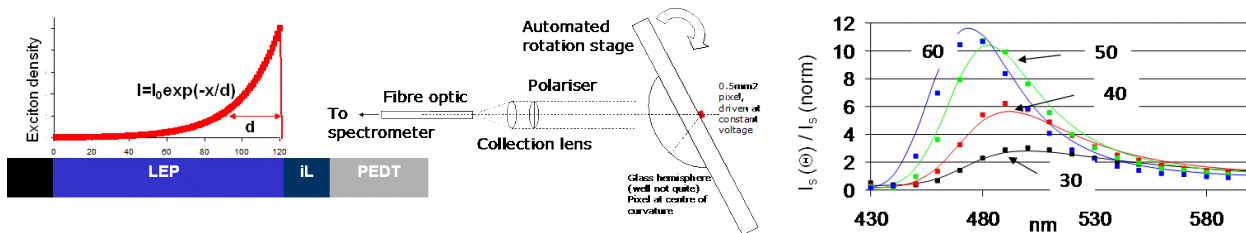


Fig. 11. PGZ measurement setup and fitting procedure. The s polarized angular emission is ratioed to its value at normal incidence. We find that for a 100-160nm thick LEP, the off axis emission spectrum accessible by using a glass hemisphere becomes extremely sensitive to the PGZ profile, and fits very well to an exponentially decaying function within the LEP peaking at the LEP:iL interface. The experimental data (dots) shown on the right hand plot is for a 130nm thick LEP device with model materials driven at 200mA/cm2 and fits very well to a PGZ profile width 16nm and peak 128nm from cathode.

The fit to the data in figure 11 is for a 130nm thick LEP device with model materials driven at 200mA/cm<sup>2</sup>. In figure 12 the results for this structure over a range of current densities are compared to the electrical model. The data gives very good fits to exponentially decaying PGZ profiles of widths between 15-25nm. Measurements at lower brightness were prevented by signal to noise issues, but the trend of narrowing RZ profile with increasing current density is in very good agreement with predictions for exciton formation zone from the electrical model. The discrepancy of about 10nm and the saturation at ~15nm can be understood by the fact that our electrical model does not take into account exciton diffusion processes, and only predicts where the excitons are formed. The PGZ measurement on the other hand measures the emission profile, after the excitons have had time to diffuse. The discrepancy between the two values is consistent with

an exciton diffusion length of order 10nm. We conclude that the PGZ profile trends measured are in reasonable agreement with our model predictions.

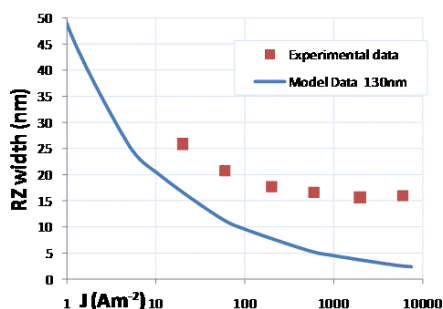


Figure 12. PGZ profile results vs current density for a 130nm thick LEP bilayer device. The general trend of narrowing PGZ profile with increasing current density is in good agreement with model predictions.

### 3.6 Dipole orientation measurements

We mentioned in the previous section that the s-polarised emission spectra only were used in the PGZ fitting procedure. Once the PGZ is fixed, then fitting the angular p polarized emission spectra can be achieved by varying a single parameter - the dipole orientation. We are effectively looking at the relative contributions of the p polarized emission from the parallel versus perpendicularly oriented dipoles. We use the same fitting procedure as for the PGZ profile, this time normalizing the p polarized spectra to the spectrum at normal incidence. We then fit for dipole orientation using a single parameter  $\alpha = k_z/k_x$ , describing the ratio of in-plane to out of plane dipoles (where the average dipole orientation is described by the vector  $(k_x, k_y, k_z)$ ). Using this method we estimate that the average dipole orientation is (0.42, 0.42, 0.16). In this notation isotropic dipoles are represented by (0.33, 0.33, 0.33) and fully in-plane dipoles by (0.5, 0.5, 0).

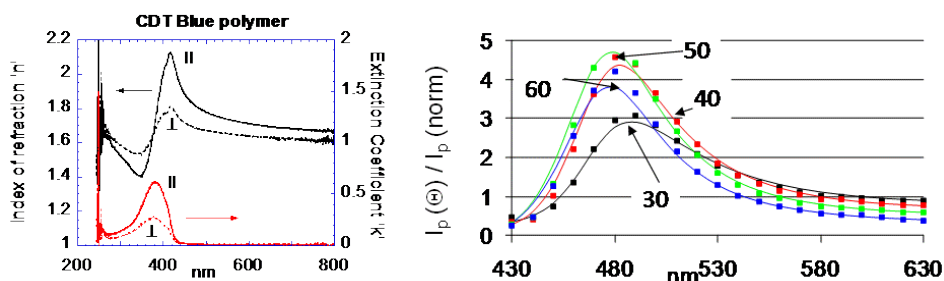


Figure 13. Dipole orientation measurements obtained for absorption via spectroscopic ellipsometry (left) and for emission from fitting of p-polarised angular emission analysis of 130nm thick LEP devices (right)

The optical modeling results from section 1 suggest that none of the perpendicular dipoles are coupled into air in a standard device structure. Interestingly we find that the values obtained are in very good agreement with the values obtained from spectroscopic ellipsometry. Using the method described by Ramsdale and Greenham<sup>10</sup> we obtain a clear signature of anisotropy in the absorption spectrum, as shown by the anisotropic extinction coefficient  $k$  in figure 13. The values obtained for the model LEP are (0.4, 0.4, 0.2). Such good agreement between the absorption and emission dipole orientations is not automatically to be expected, in particular since the absorption is dominated by the 95% F8 units, and the emission is dominated by the 5% amine units with lower exciton energy. This observation may give us interesting insights into the nature of the PFB exciton – in particular that it would appear to have significant fluorene character. This will be discussed elsewhere in future work.

### 3.7 Model material EQE with vs without iL

In the previous subsections we have presented experimental data suggesting that the model materials set satisfy the electron and hole mobility requirements for optimum exciton formation zone position. In this final subsection we present device IVL data from the model materials set (figure 14) and demonstrate that the model materials set can indeed give a high efficiency (5% EQE) at a deep blue colour point (CIEy~0.13). We also show the importance of the interlayer in achieving this efficiency, in agreement with the expectations from the simulations.

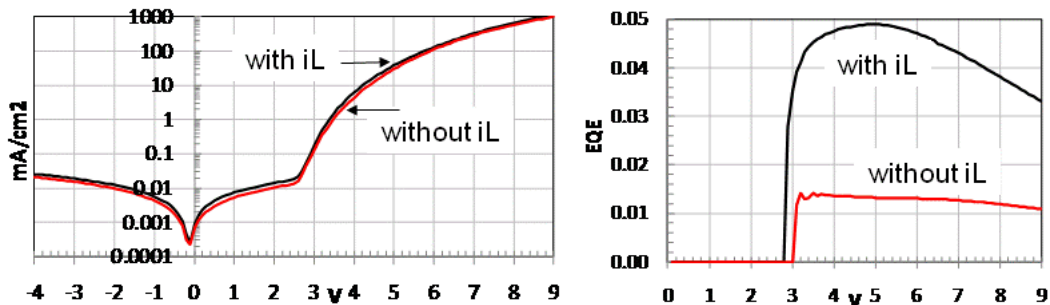


Figure 14. Device IVL using model materials set. The layer thicknesses are 60nm LEP and 15nm iL.

## 4. DEGRADATION ANALYSIS

Operational stability is of crucial importance for the commercial adoption of P-OLED technology. The figure of merit often adopted for the evaluation of operational stability is T50, defined as the time it takes for the current efficiency (cd/A) to drop to half its initial value during constant current DC operation. A typical value for the initial brightness is 1000cd/m<sup>2</sup>, and a typical lifetrace is shown in figure 15. The following section describes a degradation analysis of a device with model materials, and highlights the generation of fluorescence quenching sites as the key factor limiting the stability of these model materials. We show that this degradation has a reversible component that is even more dominant in a much improved materials set, demonstrating that understanding and prevention of this reversible component of the degradation is key to achieving longer device lifetimes.

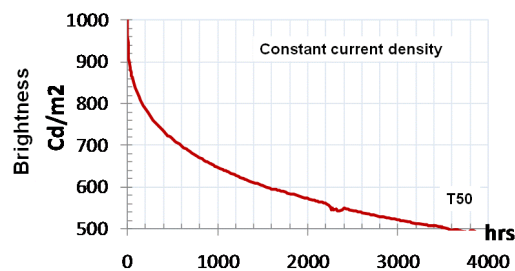


Figure 15. Lifetesting characteristic of P-OLED fluorescent blue materials. T50 is defined as the time taken for the current efficiency to drop to half its initial value.

### 4.1 Generation of fluorescence quenching sites during lifetest

Analysis of the fluorescence excited by UV (PL) at T50 for the bipolar device reveals approximately a 30% drop in the fluorescence intensity. Reverse engineering and cathode reflectance measurements (not shown) confirm that this drop in PL is a real change in the material PLQE, and not due to changes in cathode or cavity effects. The difference in the PGZs for the electrical (cd/A) and optical (PL) efficiency measurements could result in the 30% drop in PL observed being an underestimate of the local PL drop at the EL PGZ. The generation of fluorescence quenching sites is therefore the dominant factor explaining the loss in efficiency.

The fluorescence efficiency from single carrier devices is shown to be remarkably stable in comparison to the bipolar devices (figure 16). The electron only devices (semi-transparent aluminium anode) and hole only devices (aluminium cathode) can pass a charge fluence orders of magnitude greater than that passed by the bipolar devices without any measurable drop in the fluorescence intensity. This strongly suggests that the excitons themselves are involved in the degradation mechanism.

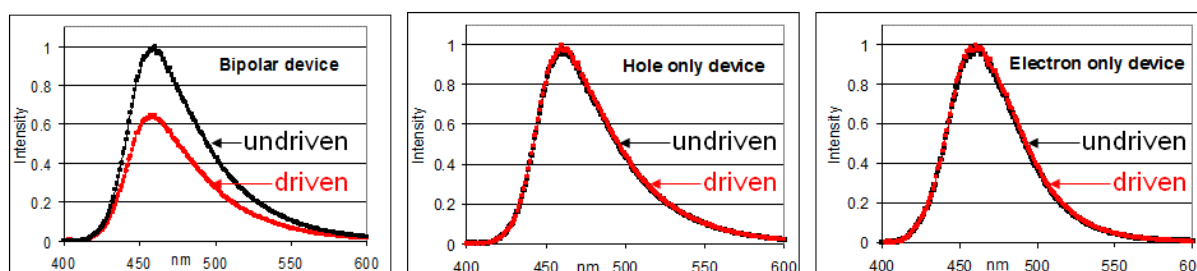


Figure 16. Fluorescence intensity of bipolar (left), hole only (centre) and electron only (right) after constant current driving. The bipolar device was driven to T50, and the single carrier device passed an equivalent amount of charge fluence. Generation of fluorescence quenching sites only occurs in the presence of excitons.

#### 4.2 Reversibility of the degradation mechanism

There are many reports of reversible degradation mechanisms in organic devices<sup>28,29</sup>. Here we report evidence of a reversible degradation in our model P-OLED devices. If a device is left at room temperature, no recovery is observed for periods >6months. However, we have found that a significant portion of the fluorescence decay can be reversed, or ‘healed’, by baking the devices in an oven. The encapsulation used was ensured to be robust to such a treatment, in that the PL of the undriven devices was not significantly changed by this process. The recovery in the PL is demonstrated in figure 17, where we plot the relative change in PL of a driven versus an undriven pixel as the temperature is slowly increased. This measurement was done with a fluorescence microscope, exciting and monitoring the PL from the pixels mounted on a hotstage. Interestingly, we found a clear threshold behavior, below which no PL was recovered. Comparison of two different materials showed that the characteristic temperature matches very well with the glass transition temperature of the LEP. This suggests to us a strong link between the recovery process and some conformational changes in the LEP.

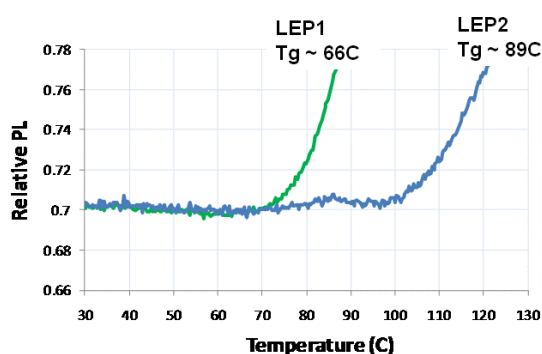


Figure 17. Relative fluorescence intensity of driven:undriven pixels as the temperature of the hotstage is slowly increased for two different LEP materials. The onset of the PL recovery process coincides with the glass transition temperature of the LEP.

This recovery in the optically excited PL efficiency is matched by a recovery in the electrically driven EL efficiency as shown in figure 18, confirming PL decay as having a direct link to the EL decay. Note that the fluorescence efficiency of undriven devices is unaffected by the baking procedure, confirming that this is truly a real recovery effect. Figure 18 shows that in the model devices, about 40% of the PL and EL degradation is recovered after baking the devices for 30mins at 120C (above Tg).

Using a combination of constant current lifetesting and baking, we are able to demonstrate that it is possible to cycle through degradation and recovery processes many times. The results in Figure 19 show the lifetraces for model devices driven for 1hour at constant current, then taken off for a 30minute bake and then put straight back on the lifetest channel at the same current. The kink showing up in the luminance after 1hr is due to the recovery of the cd/A efficiency occurring during the bake process. The process is repeated after 2 hours, where a similar recovery effect is seen. Further tests (not shown) demonstrate that this degradation and recovery process can be cycled many more times. The PL degradation process in the model devices can be divided into permanent and recoverable components. The permanent portion dominates the degradation in this case. Note that the characteristic lifetime of the recoverable degradation is similar after first and second bakes, suggesting that intrinsic stability of the recoverable portion of degradation indeed reverts back to its pristine condition and not to some weakened intermediate state.

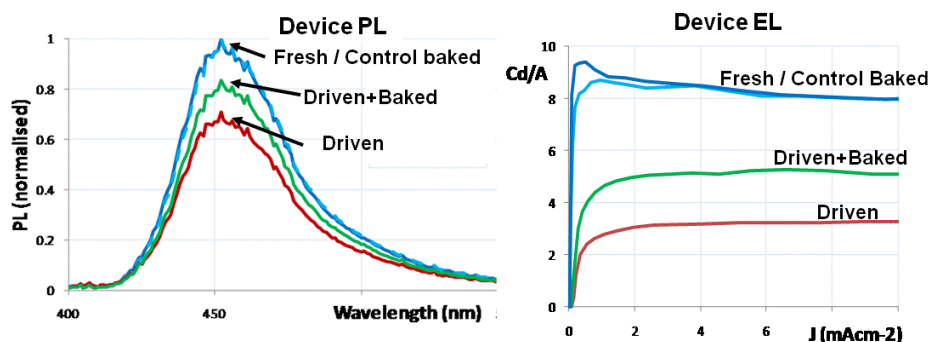


Figure 18. Baking devices at 120C for 30mins after lifetest results in a recovery of the PL (left) and also in the EL (right) efficiency. The control devices (undriven) are unaffected by the baking treatment.

Also of interest are the observed changes in the drive voltage. Similarly to the PL decay, it appears that the changes in conductivity also can be split into a permanent and a recoverable portion. This close correlation between the recoverable PL decay and the conductivity suggests a common origin – ie that the fluorescence quenching sites also affect the device conductivity.

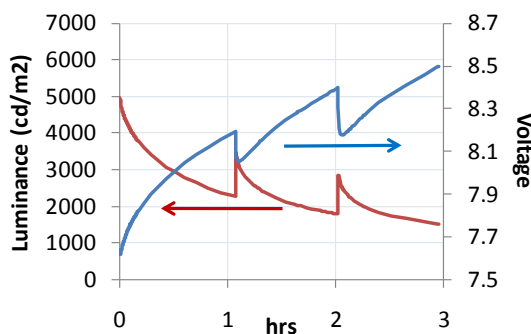


Figure 19. Cycling between degradation by constant current driving and recovery by thermal annealing, demonstrating that the reversible degradation can occur many times, and also affects the device conductivity. The kinks at 1 and 2 hours occur when the device is provisionally removed from the lifetest equipment for a 30minute bake at 120C.

### 4.3 UV exposure as a model degradation process

The lack of PL decay in single carrier devices (see section 4.1) suggests that the excitons themselves are sufficient to induce the formation of PL quenching sites. Further evidence for this can be obtained by a degradation analysis of optically (UV) excited LEP devices as shown in figure 20. For simplicity we take an LEP only device (no iL) for this demonstration so there is no ambiguity in which layer the quenching sites are formed. Instead of driving the devices electrically, the entire pixel is exposed to intense UV radiation using an array of UV photodiodes (~1W/cm<sup>2</sup>@405nm) for 3 days. We find that the fluorescence intensity can be reduced by ~30% over this period, without any significant change in the emission spectrum, similar to the level of drop expected in a driven bilayer device. We note that this degradation cannot be explained by well known photooxidation effects, as this would show up clearly as a prominent

green shoulder characteristic of fluorenone<sup>8</sup>. The device EL efficiency drops by a significant amount as a result of this treatment, depending on the current density specified. The device conductivity is also reduced; we observe a 1V increase at 10mA/cm<sup>2</sup>. Baking the degraded pixels at 120C for 30mins gives a dramatic recovery in the PL, EL and drive voltage characteristics. The recovery of the PL is nearly complete, suggesting that in this case, the majority of the fluorescence quenching sites can be recovered by baking. The significant recovery of the conductivity also confirms the strong correlation between PL decay and the voltage rise effects.

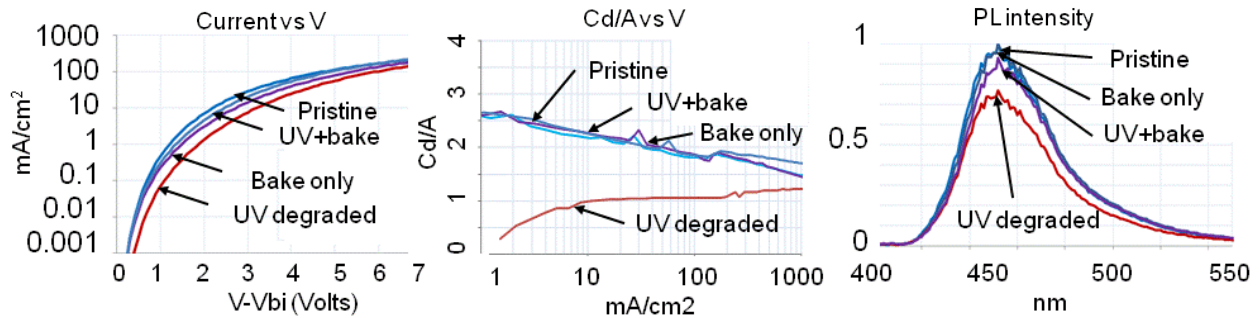


Figure 20. Degradation (by intense UV illumination) and recovery (by thermal annealing) of a single layer (LEP only) device. The optically generated excitons can generate reversible optical and electrical effects. The illumination was done with an array of UV diodes at 405nm with estimated power density of ~1W/cm<sup>2</sup> over 3 days.

Further evidence that UV excitation is a good model for degradation can be obtained by looking at photodegradation of LEP films only, in the absence of all other layers in the device as shown in figure 21. If care is taken to ensure that the films are adequately encapsulated, then we can demonstrate similar PL drops and recovery effects as seen in devices in isolated films of the LEP material only. This ability to eliminate all the other layers yet observe similar phenomena suggests that this degradation mechanism is truly an intrinsic feature of the materials, and does not require diffusion of impurities or interfacial effects that might be suspected of causing degradation in the device environment.

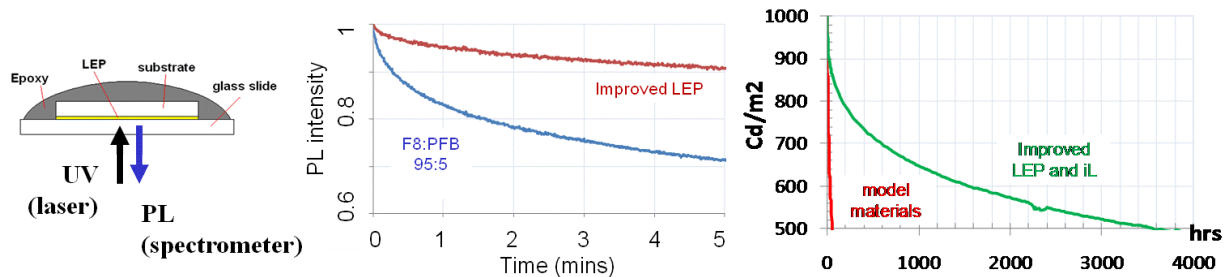


Figure 21. UV degradation of isolated films of LEP material schematic of method (left) and comparison of PL stability of model materials versus improved materials under same UV dose (centre). Improved materials excited at the same UV dose give a much improved stability to photogenerated excitons. This improvement is reflected in the equivalent device stability (right)

Also shown in figure 21 is a dramatic improvement in PL stability for an improved materials set (structures not disclosed). These materials show an improvement of over an order of magnitude in device lifetime compared to the model materials presented in this paper. Of particular interest is that similar levels of PL degradation (~30%) are observed at T50 for both the model and improved materials set, suggesting that the degradation mechanism shows some similarities, but can be slowed down considerably by material design.

#### 4.4 Recoverability of model vs improved materials

We have noted that the recoverable portion of the degradation only accounts for ~40% of the PL decay for the model materials set. In figure 22 we compare this value with the improved material set that gives over an order of magnitude improvement in lifetime. In the more modern materials set, the recoverable portion is clearly dominant, suggesting that the materials progress has come via two routes; near elimination of the permanent PL degradation mechanism, and significant slowing down of the reversible PL decay mechanism. We anticipate that further slowing down and ultimately

elimination of the reversible portion of the PL decay is a promising route for further improvement of LEP material stability.

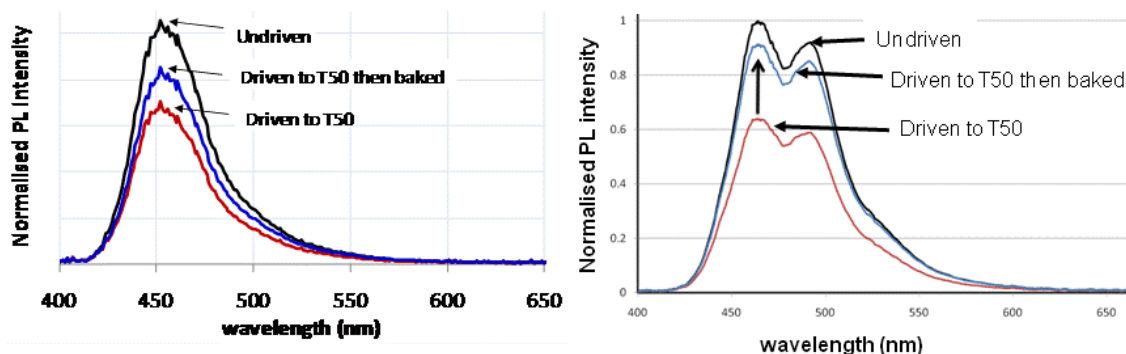


Figure 22. Recoverable fluorescence from devices with model materials (left) vs improved stability materials (right). Bilayer devices were driven to T50 and then baked at 120C for 30minutes. The proportion of the recoverable fluorescence is increased from ~40% in the model materials to >90% in the improved materials.

## 5. CONCLUSION

A detailed electrical and optical model study of bilayer P-OLED devices have revealed a number of important material and device parameters necessary to achieve good efficiency and lifetime. Most importantly for outcoupling is to ensure that the PGZ is ~55nm from a highly reflective cathode and that the dipoles are parallel to the plane. Once injection barriers are lowered for acceptable drive voltage, the LEP and iL electron and hole mobilities becomes the key factors in optimizing the exciton formation zone profile to be within the LEP and peaking at the iL:LEP interface, which can be achieved provided  $\mu_h(\text{LEP}) < \mu_e(\text{iL}) < \mu_e(\text{LEP}) < \mu_h(\text{iL})$ . Experimental data presented on our model materials gives good agreement with these model predictions.

A detailed degradation study of the model materials highlights the generation of fluorescence quenching sites as the key factor limiting the operational stability. A striking feature of this degradation is its partial (~50%) reversibility upon baking above the LEP glass transition temperature. Some of the reversibility is also observed in the conductivity, suggesting a common origin to the reversible components of optical and electrical degradation. We also show that the reversible PL quenching sites can be generated by excitons, and that optical excitation (via intense UV exposure) can also generate many of the features of normal operational lifetesting. Finally we demonstrate that materials with a dramatically improved lifetime also suffer from a similar, although slowed down, degradation mechanism, where the reversible component is increased to >90% of the quenching sites produced. This highlights the importance of understanding these reversible phenomena in improving P-OLED lifetime and commercial adoption of the technology.

## 6. REFERENCES

- [1] Bidd, I., "Designing P-OLED devices and material structures for low power consumption applications," Proceedings of AM-FPD5-8 (2009).
- [2] Lu, M.H., and Sturm, J.C., "Optimization of external coupling and light emission in organic light-emitting devices: modeling and experiment," Journal of Applied Physics 91, 595 (2002).
- [3] Ruhstaller, B., Beierlein, T., Riel, H., Karg, S., Scott, J.C., and Riess, W., "Simulating electronic and optical processes in multilayer organic light-emitting devices," IEEE Journal of Selected Topics in Quantum Electronics 9(3), 723–731 (2003).
- [4] Blom, P.W., and De Jong, M.J., "Electrical characterization of polymer light-emitting diodes," IEEE Journal of Selected Topics in Quantum Electronics 4(1), 105–112 (1998).
- [5] Coehoorn, R., Vulto, S., van Mensfoort, S.L.M., Billen, J., Bartyzel, M., Greiner, H., and Assent, R., "Measurement and modeling of carrier transport and exciton formation in blue polymer light emitting diodes (Proceedings Paper)."
- [6] Kim, J.S., Friend, R.H., Grizzi, I., and Burroughes, J.H., "Spin-cast thin semiconducting polymer interlayer for improving device efficiency of polymer light-emitting diodes," Applied Physics Letters 87, 023506 (2005).

- [7] Yang, X.H., Jaiser, F., Stiller, B., Neher, D., Galbrecht, F., and Scherf, U., "Efficient Polymer Electrophosphorescent Devices with Interfacial Layers," *Advanced Functional Materials* 16(16), 2156-2162 (2006).
- [8] Bliznyuk, V.N., Carter, S.A., Scott, J.C., Klarnar, G., Miller, R.D., and Miller, D.C., "Electrical and Photoinduced Degradation of Polyfluorene Based Films and Light-Emitting Devices," *Macromolecules* 32(2), 361-369 (1999).
- [9] Whittaker, D.M., and Culshaw, I.S., "Scattering-matrix treatment of patterned multilayer photonic structures," *Physical Review B* 60(4), 2610-2618 (1999).
- [10] Ramsdale, C., and Greenham, N., "Ellipsometric Determination of Anisotropic Optical Constants in Electroluminescent Conjugated Polymers," *Advanced Materials* 14(3), 212-215 (2002).
- [11] Adawi, A.M., Roberts, M., Connolly, L.G., Kullock, R., Turner, J.L., Smith, E., Foden, C., Qureshi, F., Athanassopoulou, N., et al., "Improving the light extraction efficiency of polymer LEDs using microcavities and photonic crystals (Proceedings Paper)."
- [12] Barnes, W.L., "Topical review. Fluorescence near interfaces: the role of photonic mode density," *J. Mod. Opt* 45(4), 661-699 (1998).
- [13] Barker, J.A., Ramsdale, C.M., and Greenham, N.C., "Modeling the current-voltage characteristics of bilayer polymer photovoltaic devices," *Physical Review B* 67(7), 075205 (2003).
- [14] Martin, S.J., Walker, A.B., Campbell, A.J., and Bradley, D.D.C., "Electrical transport characteristics of single-layer organic devices from theory and experiment," *Journal of Applied Physics* 98, 063709 (2005).
- [15] Scott, J.C., "Metal-organic interface and charge injection in organic electronic devices," *Journal of Vacuum Science & Technology A: Vacuum, Surfaces, and Films* 21, 521 (2003).
- [16] Arkhipov, V.I., Emelianova, E.V., and Bäessler, H., "Charge carrier transport and recombination at the interface between disordered organic dielectrics," *Journal of Applied Physics* 90(5), 2352 (2001).
- [17] Khan, R.U.A., Poplavskyy, D., Kreouzis, T., and Bradley, D.D.C., "Hole mobility within arylamine-containing polyfluorene copolymers: A time-of-flight transient-photocurrent study," *Physical Review B* 75(3), 035215 (2007).
- [18] van Mensfoort, S.L.M., Vulto, S.I.E., Janssen, R.A.J., and Coehoorn, R., "Hole transport in polyfluorene-based sandwich-type devices: Quantitative analysis of the role of energetic disorder," *Physical Review B* 78(8), 085208 (2008).
- [19] Campbell, A.J., Bradley, D.D.C., and Antoniadis, H., "Quantifying the efficiency of electrodes for positive carrier injection into poly(9,9-dioctylfluorene) and representative copolymers," *Journal of Applied Physics* 89(6), 3343 (2001).
- [20] Martens, H.C.F., Brom, H.B., and Blom, P.W.M., "Frequency-dependent electrical response of holes in poly(p-phenylene vinylene)," *Physical Review B* 60(12), R8489 (1999).
- [21] Fong, H.H., Papadimitratos, A., Hwang, J., Kahn, A., and Malliaras, G.G., "Hole Injection In A Model Fluorene-tertiaryamine Copolymer," *Advanced Functional Materials* 19(2), 304-310 (2009).
- [22] Harding, M.J., Poplavskyy, D., Choong, V., So, F., and Campbell, A.J., "Variations in Hole Injection due to Fast and Slow Interfacial Traps in Polymer Light-Emitting Diodes with Interlayers," *Advanced Functional Materials* 20(1), 119-130 (2010).
- [23] Takeda, N., Asaoka, S., and Miller, J.R., "Nature and energies of electrons and holes in a conjugated polymer, polyfluorene," *J. Am. Chem. Soc* 128(50), 16073-16082 (2006).
- [24] Szeghalmi, A.V., Erdmann, M., Engel, V., Schmitt, M., Amthor, S., Kriegisch, V., Noll, G., Stahl, R., Lambert, C., et al., "How Delocalized Is N, N, N, N-Tetraphenylphenylenediamine Radical Cation? An Experimental and Theoretical Study on the Electronic and Molecular Structure," *J. Am. Chem. Soc* 126(25), 7834-7845 (2004).
- [25] van Mensfoort, S.L.M., Billen, J., Vulto, S.I.E., Janssen, R.A.J., and Coehoorn, R., "Electron transport in polyfluorene-based sandwich-type devices: Quantitative analysis of the effects of disorder and electron traps," *Physical Review B* 80(3), 33202 (2009).
- [26] Granlund, T., Pettersson, L.A.A., and Inganäs, O., "Determination of the emission zone in a single-layer polymer light-emitting diode through optical measurements," *Journal of Applied Physics* 89(11), 5897 (2001).
- [27] Kim, J.S., Ho, P.K., Greenham, N.C., and Friend, R.H., "Electroluminescence emission pattern of organic light-emitting diodes: Implications for device efficiency calculations," *Journal of Applied Physics* 88, 1073 (2000).
- [28] Kawano, K., and Adachi, C., "Evaluating Carrier Accumulation in Degraded Bulk Heterojunction Organic Solar Cells by a Thermally Stimulated Current Technique," *Advanced Functional Materials* 19(24), 3934-3940 (2009).
- [29] Kobrin, P., Fisher, R., and Gurrola, A., "Reversible photodegradation of organic light-emitting diodes," *Applied Physics Letters* 85(12), 2385 (2004).

C|D|T